



THE UNIVERSITY *of* EDINBURGH

Edinburgh Research Explorer

CO₂brine substitution effects on ultrasonic wave propagation through sandstone with oblique fractures

Citation for published version:

Falconsuarez, IH, Papageorgiou, G, Jin, Z, Muñozibáñez, A, Chapman, M & Best, AI 2020, 'CO₂brine substitution effects on ultrasonic wave propagation through sandstone with oblique fractures', *Geophysical Research Letters*. <https://doi.org/10.1029/2020GL088439>

Digital Object Identifier (DOI):

[10.1029/2020GL088439](https://doi.org/10.1029/2020GL088439)

Link:

[Link to publication record in Edinburgh Research Explorer](#)

Document Version:

Peer reviewed version

Published In:

Geophysical Research Letters

Publisher Rights Statement:

©2020 American Geophysical Union. All rights reserved.

General rights

Copyright for the publications made accessible via the Edinburgh Research Explorer is retained by the author(s) and / or other copyright owners and it is a condition of accessing these publications that users recognise and abide by the legal requirements associated with these rights.

Take down policy

The University of Edinburgh has made every reasonable effort to ensure that Edinburgh Research Explorer content complies with UK legislation. If you believe that the public display of this file breaches copyright please contact openaccess@ed.ac.uk providing details, and we will remove access to the work immediately and investigate your claim.



Falcon-Suarez Ismael Himar (Orcid ID: 0000-0001-8576-5165)

Muñoz-Ibáñez Andrea (Orcid ID: 0000-0001-9107-7879)

Best Angus I. (Orcid ID: 0000-0001-9558-4261)

CO₂-brine substitution effects on ultrasonic wave propagation through sandstone with oblique fractures

By

Ismael Himar Falcon-Suarez^{1*}

Giorgos Papageorgiou^{2,3}

Zhaoyu Jin²

Andrea Muñoz-Ibáñez⁴

Mark Chapman²

&

Angus I. Best¹

(1) National Oceanography Centre, University of Southampton Waterfront
Campus. European Way, SO14 3ZH, Southampton, United Kingdom.

(2) School of Geosciences, University of Edinburgh, Grant Institute, West Mains
road, Edinburgh EH9 3FE, UK

(3) Institute of Geoscience and Petroleum, NTNU, S. P. Andersensvei 15A, 7491,
Trondheim, Norway

This article has been accepted for publication and undergone full peer review but has not been through the copyediting, typesetting, pagination and proofreading process which may lead to differences between this version and the Version of Record. Please cite this article as doi: 10.1029/2020GL088439

(4) School of Civil Engineering, University of A Coruña, Campus de Elviña s/n,
15071 A Coruña, Spain

*Corresponding author: National Oceanography Centre, University of Southampton
Waterfront Campus. European Way, SO14 3ZH, Southampton.

Phone: +44 (0)23 8059 6666 Office: 786/15 e_mail: isfalc@noc.ac.uk

Key points:

Controlled CO₂-brine flow-through test with geophysical monitoring in fractured sandstone

P-wave velocity provides more reliable information about CO₂ content than shear wave anisotropy

Elastic properties behave differently during CO₂ storage injection (drainage) and post-injection (imbibition) stages

Abstract

Seismic monitoring of injected CO₂ plumes in fractured storage reservoirs relies on accurate knowledge of the physical mechanisms governing elastic wave propagation, as described by appropriate, validated rock physics models. We measured laboratory ultrasonic velocity and attenuation of P- and S-waves, and electrical resistivity, of a synthetic fractured sandstone with obliquely aligned (penny-shaped) fractures, undergoing a brine-CO₂ flow-through test at simulated reservoir pressure and temperature. Our results show systematic differences in the dependence of velocity and attenuation on fluid saturation between imbibition and

drainage episodes, which we attribute to uniform and patchy fluid distributions, respectively, and the relative permeability of CO₂ and brine in the rock. This behaviour is consistent with predictions from a multi-fluid rock physics model, facilitating the identification of the dispersive mechanisms associated with wave induced fluid flow in fractured systems at seismic scales.

Plain language summary

Geological carbon storage (GCS) has aroused public concerns over potential surface leakage of CO₂ from geological reservoirs, limiting the number of potential storage sites. The assessment of crack distribution and fluid dynamics is a key aspect to determine the suitability of a reservoir for CO₂ storage, but also to predict the advance of the CO₂ plume underground. This work seeks to improve the distinction between fracture anisotropy and fluid distribution patterns from geophysical data using the most common monitoring tools in the field: seismic and electromagnetic technologies.

Key words: ultrasonic waves, electrical resistivity, fractures, CO₂ storage

Introduction

From the microscopic scale to large faulting systems, cracks are present in almost every rock formation found in the Earth's crust. Anisotropic and potentially frequency dependent wave propagation are key geophysical signatures describing cracked rocks. Such properties are crucial to assess the suitability of hydrocarbon reservoirs and saline aquifers for geological carbon storage (GCS) (Chiaramonte et al., 2015; Iding & Ringrose, 2010).

Previous studies have analysed a number of factors affecting the brine-CO₂ saturation dependence in saline sandstone reservoirs - the most suitable geological context for GCS (Michael et al., 2010). These factors include the distinction between pore pressure and pore fluid distribution effects (Falcon-Suarez et al., 2016, 2017, 2018), the frequency dependence of elastic wave properties and the methodology to upscale information collected in laboratory (Lei & Xue, 2009; Mikhaltsevitch et al., 2014; Nakagawa et al., 2013), or the effect of mineralogical changes in the elastic and transport properties of the rock (Canal et al., 2013; Hangx et al., 2010, 2015; Vialle & Vanorio, 2011; Vialle et al., 2014). However, most of these studies are restricted to non-fractured rocks (Nooraiepour et al., 2018), despite the nucleation and reactivation of fractures endanger safe GCS (Rutqvist 2012; Velcin et al. 2020).

The distribution of different pore fluids is largely conditioned by reservoir heterogeneities, wettability (Al-Khdheawi et al., 2017) and saturation history (Knight & Nolen-Hoeksema, 1990). To address the uncertainties associated with CO₂-brine partially saturated fractured rocks, we need to conduct controlled experiments on samples with well-defined physical and structural properties (e.g., Amalokwu et al., 2016; Rathore et al., 1995; Tillotson et al., 2011), to generate datasets to help constrain robust rock physics models. However, fluid-dependent phenomena

dominating in laboratory observations such as frequency dependent behaviour or fluid distribution in the pore space, are rarely examined in conjunction with their intrinsic anisotropy (Amalokwu et al., 2014; Murphy, 1984).

Few rock physics theories incorporate the subtleties associated with such partially saturated cracked rocks holistically. Recently, Papageorgiou & Chapman (2017) have suggested a theory that combines uniform/patchy fluid distribution (Dutta & Odé, 1979; White, 1975) and squirt flow (Chapman, 2003; Dvorkin et al., 1995) phenomena for partially saturated isotropic rocks. Later, Jin et al. (2018) extended their work to incorporate mesoscopic flow that occurs between fractures and the pore space for anisotropic rocks. The model of Jin et al. (2018) is therefore appropriate to describe frequency dependent wave velocities of partially saturated, cracked samples. If properly calibrated, this model also could be used to describe seismic velocities obtained during and after CO₂ injection in fractured GCS reservoirs.

Here, we present a brine-CO₂ partial saturation experiment in cracked sandstone with a well-defined fracture network (cracks aligned at oblique angle), under realistic geological conditions of confining (40 MPa) and pore (10 MPa) pressure. During the test, we measured ultrasonic P- and two orthogonal S-wave velocities and attenuations, together with electrical resistivity that we used to determine the evolution of the degree of CO₂ saturation (up to ~60%, including drainage and imbibition saturation paths). We simultaneously fit ultrasonic velocities to constrain the rock physics model of Jin et al. (2018), which explains the observed anisotropic and dispersive properties, and variation with partial saturation, as well as a counterintuitive increase of the velocity despite the decrease of stiff fluid. The transport and mechanical results are assessed in Muñoz-Ibáñez et al., (2019).

Experimental procedure

We used a ~2 cm length, ~5 cm diameter synthetic sandstone core plug, containing fractures aligned at 45° from its axis. The sample was manufactured using a mixture of sand, kaolinite and sodium silica gel (Falcon-Suarez et al., 2019), but with a predetermined number of 2 mm diameter (δ), 0.2 mm thickness (τ) aluminium discs (Amalokwu et al., 2015; Tillotson et al., 2012). Once baked, the sample was immersed in an acidic bath to remove the aluminium discs, resulting in a silica-cemented sandstone with 45° aligned penny-shaped cracks. The fracture density ($\epsilon_f = 0.0298 \pm 0.0077$) and an average fracture aspect ratio ($\tau/\delta = 0.088 \pm 0.001$) were obtained from X-ray CT scan image processing (Amalokwu et al., 2015), which leads to a porosity fraction attributed to fractures of ~10% (Muñoz-Ibáñez et al., 2019).

A set of 90° bi-axial 350-ohm electrical strain gauges was epoxy-glued on the lateral side wall of the sample to measure axial and radial strains during the test. Porosity (ϕ) by He-pycnometry and permeability to nitrogen (k_{gas}) were determined under minimal confining stress (~0.5 MPa) before ($\phi_0 = 27.3 \pm 0.6\%$; $k_{gas,0} = 5.5 \pm 3.13$ mD) and after ($\phi_f = 29.6 \pm 0.7\%$; $k_{gas,f} = 12.1 \pm 3.24$ mD) the test.

The sample was subjected to steady-state brine-CO₂ flow-through (BCFT), using the experimental rig for CO₂ storage multi-flow tests described in Falcon-Suarez et al. (2017). The rig implements sensors for measuring, simultaneously, electrical resistivity and ultrasonic waves (velocity and attenuation) using the pulse echo technique (Amalokwu, 2016; Best, 1992; McCann & Sothcott, 1992). Here, we used a sensor that incorporates P- and S-wave transducers in one platen, and a single S-wave transducer in the other (all transmitting 400-1000 kHz broadband acoustic pulses). For these transducers, the velocity precision is $\pm 0.1\%$ with an

accuracy of $\pm 0.3\%$ (95% confidence), while attenuation accuracy is ± 0.2 dB/cm (Best, 1992). The S-wave transducer polarisations were aligned parallel and perpendicular to the fracture strike, measuring oblique S_1 (fast) and S_2 (slow) wave velocity and attenuation, respectively, for estimations of the shear wave anisotropy (expressed as $(n_{S1} - n_{S2}) / n_{S1}$, for a given S-wave attribute n).

The BCFT test was conducted under constant hydrostatic confining ($P_c = 40$ MPa) and pore ($P_p = 10$ MPa) pressure, at room temperature (20°C), using 3.5% NaCl synthetic brine and liquid CO_2 , and covered drainage and imbibition episodes. An overpressure limit of 2 MPa was imposed (Muñoz-Ibáñez et al., 2019), which prevents rock mechanical damage (fracture propagation) at the simulated conditions (Velcin et al., 2020). The total flow ($Q = Q_w + Q_{\text{CO}_2}$) was initially regulated in each episode ($Q < 0.5 \text{ cm}^3 \text{ min}^{-1}$), and the CO_2 fractional flow ($X_{\text{CO}_2} = Q_{\text{CO}_2}/Q$) increased in 0.2 units episodes during the drainage part of the test. After the last drainage episode, the BCFT test concluded with a 100% brine flow-through to force the natural imbibition process that occurs in saline aquifers after ceasing the CO_2 injection (Gaus, 2010).

During the test, axial and radial strains were measured continuously (every second), while ultrasonic P- and $S_{1,2}$ - wave velocities (V_P , $V_{S1,2}$) and attenuations (inverse quality factors Q_P^{-1} , $Q_{S1,2}^{-1}$), and resistivity were acquired, at least, every 0.5 times the sample pore volume ($PV \sim 10.46 \text{ cm}^3$) of flow-through. Then, using Archie's first and second laws (Archie, 1942), the bulk resistivity of porous media partially saturated with brine and CO_2 was transformed into degree of brine saturation (Carrigan et al., 2013; Falcon-Suarez et al., 2016, 2017, 2018; Muñoz-Ibáñez et al., 2019; Nakatsuka et al., 2010). For resistivity, the error increases from $<1\%$ up to 5% with resistivity and sample anisotropy (North et al., 2013). The upper value leads to a

saturation uncertainty of $\pm 5\%$, when converting resistivity into degree of saturation using Archie's approach with a saturation exponent $n = 2$, usually adopted for sandstones (Mavko et al., 2009). However, the dual porosity of our sample influences the rock wettability and the saturation history (Muñoz-Ibáñez et al., 2019). In turn, n might become variable for a given resistivity-saturation relationship, invalidating the use of Archie's law (Suman and Knight, 1997; Zhou and Stenby, 1997). To account for this, we propagate saturation error derived from $\pm 10\%$ variations in n , which covers the deviation from drainage to imbibition in non-uniform pore size distribution in water-wet samples (Suman and Knight, 1997).

After the BCFT test, the sample was cleaned with deionized water and then dried, before being saturated with CO_2 at the test conditions to collect the corresponding ultrasonic properties. Further information about the testing methodology in Falcon-Suarez et al. (2017), Muñoz-Ibáñez et al. (2019) and as supporting information in the online version of this manuscript.

Results

1.1. Ultrasonic waves

The pulse-echo method used in this study (Winkler & Plona, 1982), provides accurate measurements of ultrasonic velocities and attenuation (Amalokwu, 2016; Best, 1992; Best et al., 2007; Tillotson et al., 2011, 2012). Figure 1a shows energy dissipation related to multiple arrivals for both the P- and S-wave signals between top and base reflexion peaks (framed within the data-processing windows W1 and W2, respectively). The energy dissipation is independent of the partial saturation for S_1 and S_2 , which trends are almost identical under different partial CO_2 saturations (S_{CO_2}), while multiple internal reflections distort the signal after the first pulse. P-wave

also evidences scattering arrivals in the time between the top and base reflections, but varying with the saturation state, which magnifies the overall energy dissipation, as calculated from the reduction in amplitude of the base reflection relative to the top reflection.

The horizontal and vertical cross-sections of the fractures (Figure 1b) show local fracture propagation that in some cases can exceed original fracture length (e.g., Y3). This fracture elongation is preferentially inducing energy dissipation for S-waves, which wavelength (3 mm) is closer to the fractures length (2 mm) than that of P-waves (5 mm). Therefore, the attenuation data shown in Figure 2 have to be understood in qualitative terms, with Q_P^{-1} showing significant changes between drainage and imbibition paths, while the Q_{S1}^{-1} and Q_{S2}^{-1} are largely affected by scattering with no significant changes (i.e., variations lie within the experimental error).

1.2. BCFT test

The brine-CO₂ flow-through (BCFT) test lasted ~75 h, resulting in a total fluid throughput of ~63 PV. Figure 2 shows the ultrasonic properties (V_P , $V_{S1,2}$ and Q_P^{-1} , $Q_{S1,2}^{-1}$; all the results at 600 kHz obtained from Fourier analysis of the broadband signals), plotted together with the electrical resistivity and volumetric strains measured during the BCFT test.

The transition from the first brine:CO₂ fractional flow episode ($X_{CO_2} = 0$) to the second ($X_{CO_2} = 0.2$) marks the arrival of the free CO₂ phase in the rock (PV ~3.6), and the resistivity increases progressively with the volume of CO₂ passing through the rock. The CO₂ arrival leads to a sharp increase of V_P (~1.5%) and Q_P^{-1} (~50%), followed by a progressive decrease of V_P with the increasing CO₂ content and the opposite for Q_P^{-1} . The two orthogonal components of the shear wave show similar

trends in both the velocities (V_{S1} , V_{S2}) and the attenuations (Q_{S1}^{-1} , Q_{S2}^{-1}), with relative differences of ~6% between V_{S1} and V_{S2} and throughout the BCFT test. V_{S1} and V_{S2} drop during $X_{CO2} = 0.2$, followed by a soft increasing trend thereafter. Similarly, Q_{S1}^{-1} and Q_{S2}^{-1} progressively increase during drainage and drop to approximately the original values during the forced imbibition episode ($X_{CO2} = R-0$). However, this trend is inconclusive as it occurs within the experimental uncertainty.

The imbibition (R-0) started with a single brine pulse (~0.5 PV at 42.8 PV; BP in Figure 2), with continuous monitoring of the geophysical properties of the sample. Then, continuous brine flow through the sample was progressively replacing the CO_2 from the pore space, as inferred from the resistivity drop (down to ~24% above the original brine saturated conditions). The imbibition affected P- and S-waves properties differently: V_P increased and Q_P^{-1} decreased, both up to ~2% below and above the original brine saturated values, respectively; while $V_{S1,2}$ and $Q_{S1,2}^{-1}$ fully recovered by the end of the imbibition. Yin et al. (1992) also found that the attenuation depends not only on the degree of saturation and the frequency of the measurements, but also on the saturation history. They reported ~7% shift on the degree of saturation for the attenuation peak from drainage to imbibition paths at sonic frequencies (~1500 Hz). In our case, this shift reaches up to 30% for Q_P^{-1} (Figure 2), because of the interplay of the scattering on heterogeneities (cracks-induced internal reflections) and energy dispersive mechanisms related to partial fluid flow in porous media. This render the attenuation measurements unreliable as quantitative indicators of the changing physical properties of the sample due to pore fluid substitution.

The sample evidences mechanical deformation (inflation) after $X_{CO2} > 0.5$, which stabilizes during imbibition. This minor inflation (~0.12%) is within the porosity

fraction commonly attributed to microcracks (0.7%; Fortin et al. (2007)). Thus, it could be related to microcracks reopening due to differential pressure ($P_{\text{diff}} = P_c - P_p$) drop during the experiment associated with the increase of inlet-to-outlet P_p gradients with the increasing X_{CO_2} (Muñoz-Ibáñez et al., 2019).

Insights from data analysis

Theories for wave propagation through partially saturated rocks emphasise two dominant dispersive mechanisms taking place when wave propagation induces local and meso-scale fluid flow: squirt flow (Chapman, 2003; Dvorkin et al., 1995) and patchy saturation (Dutta & Odé, 1979; White, 1975) effects. While the diffusive character of Biot flow (Biot, 1956) is significant in unconsolidated sediments, in consolidated rocks the predicted dispersion is much smaller and occurs at much higher frequencies than the experimental frequency. We therefore focus on the first two: squirt flow and patchy saturation.

Papageorgiou & Chapman (2017) combined these two effects into a single theory. Later, Jin et al. (2018) extended their theory to include anisotropic effects due to fractures, showing that the moduli of a fractured, partially saturated rock can be interpreted as two coupled standard linear solid (SLS) models (Mavko et al., 2009). These two SLS models have relaxation frequencies linked by the scale ratio of the fracture size to the pore/microcrack size. For a rock with aligned fractures, the SLS with lower relaxation frequency corresponds to an anisotropic mechanism that induces dispersion in the fracture normal direction only, whereas the SLS with higher relaxation frequency is isotropic.

In partial saturation, both the combined squirt-patch effect and the effective fluid moduli impact the two SLS relaxation frequencies (Brie et al., 1995; Papageorgiou &

Chapman, 2017). The relaxation frequencies depend on relative permeability and a patch parameter q , which lies between 1 at uniform saturation and the ratio of the fluid moduli at patchy saturation (Papageorgiou & Chapman, 2017). The magnitude of each SLS model induced dispersion is controlled by the fracture density (ε_f) and by microcrack density (ε_m), for the SLS with lower and higher relaxation frequency, respectively.

To calculate the relaxation frequencies at partial saturation, we use the Brooks-Corey relative permeability model, suitable for explaining the two fluid phases interaction in our sample (Muñoz-Ibáñez et al., 2019), and the fracture and microcrack densities $\varepsilon_f = 0.042$ and $\varepsilon_m = 0.02$. ε_f is derived from the design of synthetic fractures in the sample (Tillotson et al., 2012), while ε_m is arbitrarily adopted within the range of values observed in similar synthetic rocks (Papageorgiou et al., 2018). In the supporting information we show how we derive the V_P , V_{S1} , V_{S2} of an effective medium with these properties. The increase in V_P at low saturation, together with the absence of fluid dependent shear wave anisotropy, is consistent with the behaviour of our model in the frequency regime, where the large fractures are effectively sealed but squirt flow dispersion is still observable isotropically. Current data prevent us from further constraining these frequencies, so we present modelling for a range of relaxation frequencies of the microcrack SLS relative to the experiment frequency, as well as saturation distribution scenarios for patchy and uniform saturated pores.

Figure 3 summarises our modelling results, considering the relaxation frequency and fluid distribution scenarios (Figure 3a) and the model's predictions for V_P , V_S and shear wave anisotropy (Figure 3b-d). For the fit, we perform a nonlinear Nelder-Mead minimization in two steps for each of the three relaxation frequencies ω_i . First,

we deduce effective medium matrix parameters λ , μ at full water saturation, i.e., we determine λ , μ given constant ϵ , ϵ_f , ω_i such that, when $S_w = 1$, $(V_{P(th)}(\lambda, \mu) -$

$V_{P(ex)})^2 + (V_{S1(th)}(\lambda, \mu) - V_{S1(ex)})^2 + (V_{S2(th)}(\lambda, \mu) - V_{S2(ex)})^2$ is minimum (subscripts *th* and *ex* for theoretic and experimental, respectively). As a second step, we invert for the patch parameter at partial saturation for each of the imbibition/drainage stages, i.e.

given λ , μ , ϵ , ϵ_f , ω_i , we determine q such that $\sum_{S_j} ((V_{P(theor)}(q) -$

$V_{P(exp)})^2 + (V_{S1(theor)}(q) - V_{S1(exp)})^2 + (V_{S2(theor)}(q) - V_{S2(exp)})^2$ is minimum, where S_j are the saturation steps for which we have data.

Despite the difference in fluids and incomplete saturation path, our V_P results are similar in form to the observations in Knight & Nolen-Hoeksema (1990), where velocities showed strong hysteresis with values consistently higher during drainage. Knight & Nolen-Hoeksema (1990) attribute this discrepancy to a difference in pore-fluid distribution under drainage (patchy saturation) and imbibition (uniform saturation), which is consistent with our observations. However, we note the lack of significant V_s hysteresis and the strong impact of the saturation distribution to the velocity dispersion in our work.

The absence of imbibition data with $S_w \geq 0.85$ prevents saturation history analysis at the high saturation regime, and indicates a residual CO_2 trapping of $\sim 15\%$ at the experimental conditions. However, the increase observed in porosity ($\sim 5\%$) and permeability ($\sim 45\%$) after the BCFT test might have occurred during drainage. Then, abnormally high values of $V_{S1,2}$ measured at full CO_2 saturation (marked by stars in Figure 3), together with the elevated $V_{S1,2}$ and reduced V_P values with respect to modelling along the imbibition path, indicate the reduction of the

sample's density (i.e., porosity increase) affected its shear modulus minimally, in agreement with Delle Piane & Sarout (2016).

We also observe a striking increase in V_P at low CO_2 saturation ($S_w \sim 0.9$), despite addition of softer fluid in the system. Given the similar density between the CO_2 and brine, this increase is attributed to an increase in the elastic modulus. This phenomenon is unusual, but still identified in previously reported data for sandstones (Batzle et al., 2006), limestones (Cadoret et al., 1995) and shales (Szewczyk et al., 2018), with air and water as pore fluids under atmospheric pressure conditions. In our experiment, the viscosity and moduli of the two fluids differ by only one or two orders of magnitude within the experimental bandwidth, which magnifies the observed effect with respect to the previous observations. This increase is also present in the modelling predictions and we have excluded CO_2 dissolution into water as a possible cause for this phenomenon as its impact would be of the order of $<1\%$, much smaller than the observation. The reason for this increase lies in the complex interplay between partial fluid mobility and effective fluid modulus: a S_w range exists between 0.8 and 0.9 in which the dispersion from frequency dependent effects overcompensates for the addition of the soft fluid, making the system stiffer at partial than at full saturation.

Discussion

The ultimate goal of our work is to understand the geophysical behaviour of fractured reservoirs undergoing CO_2 injection and identify the mechanisms that can be used to effectively monitor GCS projects. We extend the work of Nooraiepour et al. (2018) in considering properties of distributions of fractures, which is closer to the equivalent medium concept required to scale to reservoir conditions. To date, data

regarding partial saturation in fractured media are limited to controlled experiments at atmospheric conditions using water and air as non-wetting phase (e.g., Amalokwu, 2016). The air has higher compressibility, lower viscosity and density three orders of magnitude lower than ours at the experimental conditions (i.e., liquid CO₂).

Therefore, we expect to find discrepancies between our results and those found in the literature related to the non-wetting fluid properties.

The properties of the pore fluids and their mobility through the porous media complicate the distinction between pore fluid distribution and rock fabric in fractured media. Kong et al. (2017) remarked that the fracture-filling fluid can disguise P-wave dispersion and attenuation effects due to fracture orientation, when its modulus is much smaller than that of the pore-filling fluid. Amalokwu et al. (2015) found that fractures obliquely oriented respect to wave propagation can lead to S-wave velocity anisotropy (SWVA) drop with increasing water saturation, because V_{s2} (sensitive to fluid compressibility reduction) decreases; whilst V_{s1} , considered independent of the pore fluid (Tillotson et al., 2012), remains constant. Conversely, our results show minor SWVA variation with the CO₂ content, within the bounds imposed by experimental error.

The distribution of the two fluids in our porous medium is conditioned by the wettability of the CO₂-brine-rock system, the pore geometry and the saturation history (Cinar & Riaz, 2014; Krevor et al., 2015). Our experiment simulates different stages of CO₂ injection in fractured saline siliciclastic reservoirs, at realistic geological stress conditions. The test covers fluid substitution during CO₂ plume advance (drainage) and the natural aquifer recharge after ceasing the injection activities (imbibition) with a maximum CO₂ saturation ~0.6, in agreement with previous CO₂-water fluid substitution tests in sandstones (Burnside & Naylor, 2014).

The low capillarity forces of the fractures with respect to the pores leads to preferential CO₂ fracture filling (Muñoz-Ibáñez et al., 2019), which magnifies the effect of drainage versus imbibition paths.

Our results indicate that P-wave properties (V_P , Q_P^{-1}) are highly sensitive to the saturation history, while S-waves show very little differences between drainage and imbibition saturation paths. This finding has important implications for CO₂ storage, since the information inferred from seismic surveys during the injection and post-injection activities are significantly different; but this also applies for the differential monitoring of the front (drainage) and the trailing edge (imbibition) of the CO₂ plume. The degree of partial saturation in sandstones with fractures aligned at oblique angles might have some effect in the SWVA, in agreement with Amalokwu et al. (2016), but certainly insufficient to be used as a robust indicator of pore fluid distribution. This finding has direct application on the interpretation of S-wave splitting datasets from gas and GCS reservoirs containing or developing fractures during production or injection activities.

The use of ultrasonic waves to explore fractured media is influenced by the characteristics of the fracture, such as fracture length (c), aperture, crack surface roughness or the saturating fluid; also, the wavelength (λ_w). If $c/\lambda_w < 1$, the porous medium appears homogeneous; while for $c/\lambda_w > 1$, heterogeneities begin to act as energy scattering fronts. In our rock sample, c is slightly lower than λ_w for both the P- and S-waves, which leads to some wave scattering in the recorded signals. In addition, regardless how homogeneous the medium is, absolute scale also plays a part.

Here, we identify and analyse the mechanisms that are necessary to describe an effective medium that reproduces the dispersive behaviour of the rock. The

results from our controlled experiment suggest that fluid flow induces dispersive behaviour at the pore and fracture scale (with a transition frequency that scales with effective mobility), which is sufficient to describe this fractured medium. Likewise, we observe that despite the single experimental frequency, dispersion varies across saturation consistently with our modelling strategy indicating that the dominant mechanisms - at least with respect to wave induced fluid flow, have been taken into account in the effective medium. This interpretation is supported by Figure 3, where the counterintuitive features of the model are reproduced, such as the increase of compressional velocity at intermediate saturation depending on drainage/imbibition paths, in conjunction with the relatively small dispersion in shear wave velocities.

Likewise, we anticipate that a fractured, partially saturated reservoir rock will exhibit dispersive behaviour according to these mechanisms at the field scale. To make this fully predictive, we would need to calibrate the model with specific field velocity measurements and have a hydrological characterization of the reservoir formation. Our identification of these mechanisms offers a step toward overcoming the difficulty in distinguishing saturation effects from fluid distribution effects in fractured systems. This problem is dominant in the characterization and monitoring of CO₂ storage reservoirs where faults have been recognized (Chiaramonte et al., 2015; Iding & Ringrose, 2010).

Conclusions

In this work, we record experimental observation suggesting anisotropic rocks with aligned fractures have bulk and shear elastic behaviour that depends on the saturation path (imbibition/drainage). During our high pressure brine-CO₂ flow-through experiment on a synthetic sandstone, stiffening was observed for low

(~10%) CO₂ saturation in the drainage phase, despite the apparent fluid softening. We found shear wave velocity anisotropy to be independent of saturation path and were unable to draw conclusions about its dependence on fluid content due to high uncertainties associated with the S-wave measurements. Using recently published work, we were able to explain the dependence of the elastic constants on imbibition and drainage. We observe manifestations of different patchiness in the fluid distribution, with more uniform saturation during imbibition and patchy saturation during drainage, in accordance to previously published experiments performed on isotropic rocks. Using the same rock physics model, we were able to capture the increase in modulus observed during drainage as resulting from a decrease in effective mobility due to relative permeability effects.

Acknowledgments

We have received funding from the UK's Natural Environment Research Council (grant NE/R013535/1 GASRIP, and grant NE/N016041/1 CHIMNEY), the European Union's Horizon 2020 research and innovation programme (grant No. 654462 STEMM-CCS), the program PETROMAKS2 of the Research Council of Norway (RCN grant number:267765), and the Xunta de Galicia and the European Union (European Social Fund – ESF). Zhaoyu Jin was supported by the Principal's Career Development PhD Scholarship and Edinburgh Global Research Scholarship from The University of Edinburgh. The experiment was conducted at the NOC Rock Physics Laboratory in Southampton. The authors thank Dr Laurence North for his support in the laboratory with the resistivity measurements. Data presented in this study are available at the UK National Geoscience Data Centre (NGDC) repository (<https://doi.org/10.5285/abc38c58-3a69-42ed-86ac-1502509bd88c>).

Author contributions: IHFS contribution roles include conceptualization, data curation, funding acquisition, methodology, resources, supervision, validation, visualization and writing – original draft; GP contribution roles include conceptualization, formal analysis, software, supervision, validation and writing – original draft; ZJ contribution roles include formal analysis, investigation and software; AMI contribution roles include data curation and writing – review & editing; MC contribution roles include resources, software and supervision; AIB contribution roles include resources and writing – review & editing.

References

- Al-Khdheewi, E. A., Vialle, S., Barifcani, A., Sarmadivaleh, M., & Iglauder, S. (2017), Impact of reservoir wettability and heterogeneity on CO₂-plume migration and trapping capacity, *International Journal of Greenhouse Gas Control*, 58, 142-158, <https://doi.org/10.1016/j.ijggc.2017.01.012>
- Amalokwu, K. (2016), Saturation effects on frequency-dependent seismic anisotropy in fractured porous rocks, Doctoral thesis, 168 pp, University of Southampton.
- Amalokwu, K., Best, A. I., & Chapman, M. (2016), Effects of aligned fractures on the response of velocity and attenuation ratios to water saturation variation: a laboratory study using synthetic sandstones, *Geophysical Prospecting*, 64(4), 942-957, <https://doi.org/10.1111/1365-2478.12378>
- Amalokwu, K., Best, A. I., Sothcott, J., Chapman, M., Minshull, T., & Li, X.-Y. (2014), Water saturation effects on elastic wave attenuation in porous rocks with aligned fractures, *Geophysical Journal International*, 197(2), 943-947, <https://doi.org/10.1093/gji/ggu076>

Amalokwu, K., Chapman, M., Best, A. I., Sothcott, J., Minshull, T. A., & Li, X.-Y. (2015), Experimental observation of water saturation effects on shear wave splitting in synthetic rock with fractures aligned at oblique angles, *Geophysical Journal International*, 200(1), 17-24, <https://doi.org/10.1093/gji/ggu368>

Archie, G. E. (1942), The electrical resistivity log as an aid in determining some reservoir characteristics, <https://doi.org/10.2118/942054-G>

Batzle, M. L., Han, D.-H., & Hofmann, R. (2006), Fluid mobility and frequency-dependent seismic velocity-Direct measurements, *Geophysics*, 71(1), N1-N9, <https://doi.org/10.1190/1.2159053>

Best, A. I. (1992), The prediction of the reservoir properties of sedimentary rocks from seismic measurements, 393 pp, University of Reading.

Best, A. I., Sothcott, J., & McCann, C. (2007), A laboratory study of seismic velocity and attenuation anisotropy in near-surface sedimentary rocks, *Geophysical Prospecting*, 55(5), 609-625, <https://doi.org/10.1111/j.1365-2478.2007.00642.x>

Brie, A., Pampuri, F., Marsala, A. F., & Meazza, O. (1995), Shear sonic interpretation in gas-bearing sands, in *SPE Annual Technical Conference and Exhibition*, edited, p. 10, Society of Petroleum Engineers, Dallas, Texas.

Burnside, N. M., & Naylor, M. (2014), Review and implications of relative permeability of CO₂/brine systems and residual trapping of CO₂, *International Journal of Greenhouse Gas Control*, 23(0), 1-11, <http://doi.org/10.1016/j.ijggc.2014.01.013>

Cadoret, T., Marion, D., & Zinszner, B. (1995), Influence of frequency and fluid distribution on elastic wave velocities in partially saturated limestones, *Journal of Geophysical Research: Solid Earth*, 100(B6), 9789-9803, <https://doi.org/10.1029/95JB00757>

Canal, J., Delgado, J., Falcón, I., Yang, Q., Juncosa, R., & Barrientos, V. (2013), Injection of CO₂-saturated water through a siliceous sandstone plug from the Hontomin test site (Spain): Experiment and modeling, *Environmental Science & Technology*, 47(1), 159-167, <http://doi.org/10.1021/es3012222>

Carrigan, C. R., et al. (2013), Electrical resistance tomographic monitoring of CO₂ movement in deep geologic reservoirs, *International Journal of Greenhouse Gas Control*, 18(0), 401-408, <http://doi.org/10.1016/j.ijggc.2013.04.016>

Chapman, M. (2003), Frequency-dependent anisotropy due to meso-scale fractures in the presence of equant porosity, *Geophysical Prospecting*, 51(5), 369-379, <https://doi.org/10.1046/j.1365-2478.2003.00384.x>

Chiaramonte, L., White, J. A., & Trainor-Guitton, W. (2015), Probabilistic geomechanical analysis of compartmentalization at the Snøhvit CO₂ sequestration project, *Journal of Geophysical Research: Solid Earth*, 120(2), 1195-1209, <https://doi.org/10.1002/2014JB011376>

Cinar, Y., & Riaz, A. (2014), Carbon dioxide sequestration in saline formations: Part 2—Review of multiphase flow modeling, *Journal of Petroleum Science and Engineering*, 124, 381-398, <https://doi.org/10.1016/j.petrol.2014.07.023>

Delle Piane, C., & Sarout, J. (2016), Effects of water and supercritical CO₂ on the mechanical and elastic properties of Berea sandstone, *International Journal of Greenhouse Gas Control*, 55, 209-220, <http://doi.org/10.1016/j.ijggc.2016.06.001>

Dutta, N. C., & Odé, H. (1979), Attenuation and dispersion of compressional waves in fluid-filled porous rocks with partial gas saturation (White model)—Part I: Biot theory, *Geophysics*, 44(11), 1777-1788, <https://doi.org/10.1190/1.1440938>

Dvorkin, J., Mavko, G., & Nur, A. (1995), Squirt flow in fully saturated rocks, *Geophysics*, 60(1), 97-107, <https://doi.org/10.1190/1.1443767>

Falcon-Suarez, I., North, L., Amalokwu, K., & Best, A. (2016), Integrated geophysical and hydromechanical assessment for CO₂ storage: shallow low permeable reservoir sandstones, *Geophysical Prospecting*, 64(4), 828-847, <http://doi.org/10.1111/1365-2478.12396>

Falcon-Suarez, I., Papageorgiou, G., Chadwick, A., North, L., Best, A., & Chapman, M. (2018), CO₂-brine flow-through on an Utsira Sand core sample: Experimental and modelling. Implications for the Sleipner storage field, *International Journal of Greenhouse Gas Control*, 68, 236-246, <https://doi.org/10.1016/j.ijggc.2017.11.019>

Falcon-Suarez, I., Marín-Moreno, H., Browning, F., Lichtschlag, A., Robert, K., North, L. J., & Best, A. I. (2017), Experimental assessment of pore fluid distribution and geomechanical changes in saline sandstone reservoirs during and after CO₂ injection, *International Journal of Greenhouse Gas Control*, 63, 356-369, <https://doi.org/10.1016/j.ijggc.2017.06.019>

Falcon-Suarez, I. H., Amalokwu, K., Delgado-Martin, J., Callow, B., Robert, K., North, L., Sahoo, S. K., & Best, A. I. (2019), Comparison of stress-dependent geophysical, hydraulic and mechanical properties of synthetic and natural sandstones for reservoir characterization and monitoring studies, *Geophysical Prospecting*, 67(4), 784-803, <https://doi.org/10.1111/1365-2478.12699>

Fortin, J., Guéguen, Y., & Schubnel, A. (2007), Effects of pore collapse and grain crushing on ultrasonic velocities and Vp/Vs, *Journal of Geophysical Research*, 112(B8), B08207, <https://doi.org/10.1029/2005jb004005>

Gaus, I. (2010), Role and impact of CO₂-rock interactions during CO₂ storage in sedimentary rocks, *International Journal of Greenhouse Gas Control*, 4(1), 73-89, <http://doi.org/10.1016/j.ijggc.2009.09.015>

Guéguen, Y., & Schubnel, A. (2003), Elastic wave velocities and permeability of cracked rocks, *Tectonophysics*, 370(1-4), 163-176, [https://doi.org/10.1016/S0040-1951\(03\)00184-7](https://doi.org/10.1016/S0040-1951(03)00184-7)

Hangx, S., Bakker, E., Bertier, P., Nover, G., & Busch, A. (2015), Chemical–mechanical coupling observed for depleted oil reservoirs subjected to long-term CO₂-exposure – A case study of the Werkendam natural CO₂ analogue field, *Earth and Planetary Science Letters*, 428, 230-242, <http://doi.org/10.1016/j.epsl.2015.07.044>

Hangx, S. J. T., Spiers, C. J., & Peach, C. J. (2010), Creep of simulated reservoir sands and coupled chemical-mechanical effects of CO₂ injection, *Journal of Geophysical Research: Solid Earth*, 115(B9), B09205, <http://doi.org/10.1029/2009JB006939>

Iding, M., & Ringrose, P. (2010), Evaluating the impact of fractures on the performance of the In Salah CO₂ storage site, *International Journal of Greenhouse Gas Control*, 4(2), 242-248, <https://doi.org/10.1016/j.ijggc.2009.10.016>

IPCC (2005), *IPCC Special Report on Carbon Dioxide Capture and Storage*. Prepared by Working Group III of the Intergovernmental Panel on Climate Change. Metz, B., O. Davidson, H. C. de Coninck, M. Loos, and L. A. Meyer (eds.). Cambridge University Press, Cambridge, United Kingdom and New York, NY, USA, 442 pp.

Jin, Z., Chapman, M., & Papageorgiou, G. (2018), Frequency-dependent anisotropy in a partially saturated fractured rock, *Geophysical Journal International*, 215(3), 1985-1998, <https://doi.org/10.1093/gji/ggy399>

Knight, R., & Nolen-Hoeksema, R. (1990), A laboratory study of the dependence of elastic wave velocities on pore scale fluid distribution, *Geophysical Research Letters*, 17(10), 1529-1532, <https://doi.org/10.1029/GL017i010p01529>

Kong, L., Gurevich, B., Zhang, Y., & Wang, Y. (2017), Effect of fracture fill on frequency-dependent anisotropy of fractured porous rocks, *Geophysical Prospecting*, 65(6), 1649-1661, <https://doi.org/10.1111/1365-2478.12505>

Krevor, S., Blunt, M. J., Benson, S. M., Pentland, C. H., Reynolds, C., Al-Menhali, A., & Niu, B. (2015), Capillary trapping for geologic carbon dioxide storage – From pore scale physics to field scale implications, *International Journal of Greenhouse Gas Control*, 40, 221-237, <http://doi.org/10.1016/j.ijggc.2015.04.006>

Lei, X., & Xue, Z. (2009), Ultrasonic velocity and attenuation during CO₂ injection into water-saturated porous sandstone: Measurements using difference seismic tomography, *Physics of The Earth and Planetary Interiors*, 176(3:4), 224-234, <https://doi.org/10.1016/j.pepi.2009.06.001>

Mavko, G., Mukerji, T., & Dvorkin, J. (2009), *Rock physics handbook - Tools for seismic analysis in porous media*, Cambridge University Press, New York.

McCann, C., & Sothcott, J. (1992), Laboratory measurements of the seismic properties of sedimentary rocks, *Geological Society, London, Special Publications*, 65(1), 285-297, <https://doi.org/10.1144/gsl.sp.1992.065.01.22>

Michael, K., Golab, A., Shulakova, V., Ennis-King, J., Allinson, G., Sharma, S., & Aiken, T. (2010), Geological storage of CO₂ in saline aquifers: A review of the experience from existing storage operations, *International Journal of Greenhouse Gas Control*, 4(4), 659-667, <http://doi.org/10.1016/j.ijggc.2009.12.011>

Mikhailsevitch, V., Lebedev, M., & Gurevich, B. (2014), Measurements of the elastic and anelastic properties of sandstone flooded with supercritical CO₂, *Geophysical Prospecting*, 62(6), 1266-1277, <https://doi.org/10.1111/1365-2478.12181>

Muñoz-Ibáñez, A., Falcon-Suarez, I. H., Marín-Moreno, H., Martín, J. D., & Mackin, P. (2019), Transport properties of saline CO₂ storage reservoirs with unconnected fractures from brine-CO₂ flow-through tests, *Journal of Petroleum Science and Engineering*, 106551, <https://doi.org/10.1016/j.petrol.2019.106551>

Murphy, W. F. (1984), Acoustic measures of partial gas saturation in tight sandstones, *Journal of Geophysical Research: Solid Earth*, 89(B13), 11549-11559, <https://doi.org/10.1029/JB089iB13p11549>

Nakagawa, S., Kneafsey, T. J., Daley, T. M., Freifeld, B. M., & Rees, E. V. (2013), Laboratory seismic monitoring of supercritical CO₂ flooding in sandstone cores using the Split Hopkinson Resonant Bar technique with concurrent x-ray Computed Tomography imaging, *Geophysical Prospecting*, 61(2), 254-269, <https://doi.org/10.1111/1365-2478.12027>

Nakatsuka, Y., Xue, Z., Garcia, H., & Matsuoka, T. (2010), Experimental study on CO₂ monitoring and quantification of stored CO₂ in saline formations using resistivity measurements, *International Journal of Greenhouse Gas Control*, 4(2), 209-216, <http://doi.org/10.1016/j.ijggc.2010.01.001>

Nooraiepour, M., Bohloli, B., Park, J., Sauvin, G., Skurtveit, E., & Mondol, N. H. (2018), Effect of brine-CO₂ fracture flow on velocity and electrical resistivity of naturally fractured tight sandstones, *Geophysics*, 83(1), WA37-WA48, <https://doi.org/10.1190/geo2017-0077.1>

North, L., Best, A. I., Sothcott, J., & MacGregor, L. (2013), Laboratory determination of the full electrical resistivity tensor of heterogeneous carbonate rocks at elevated pressures, *Geophysical Prospecting*, 61(2), 458-470, <https://doi.org/10.1111/j.1365-2478.2012.01113.x>

Papageorgiou, G., & Chapman, M. (2017), Wave-propagation in rocks saturated by two immiscible fluids, *Geophysical Journal International*, 209(3), 1761-1767, <https://doi.org/10.1093/gji/ggx128>

Rathore, J. S., Fjaer, E., Holt, R. M., & Renlie, L. (1995), P- and S-wave anisotropy of a synthetic sandstone with controlled crack geometry, *Geophysical Prospecting*, 43(6), 711-728, <https://doi.org/10.1111/j.1365-2478.1995.tb00276.x>

Rutqvist, J. (2012), The geomechanics of CO₂ storage in deep sedimentary formations, *Geotechnical and Geological Engineering*, 30(3), 525-551, <http://doi.org/10.1007/s10706-011-9491-0>

Schoenberg, M., & Sayers, C. M. (1995), Seismic anisotropy of fractured rock, *Geophysics*, 60(1), 204-211, <https://doi.org/10.1190/1.1443748>

Suman, R. J., & R. J. Knight, 1997, Effects of pore structure and wettability on the electrical resistivity of partially saturated rocks—A network study, *Geophysics*, 62(4), 1151-1162, <http://dx.doi.org/10.1190/1.1444216>.

Szewczyk, D., Holt, R. M., & Bauer, A. (2018), The impact of saturation on seismic dispersion in shales — Laboratory measurements, *Geophysics*, 83(1), MR15-MR34, <https://doi.org/10.1190/geo2017-0169.1>

Tillotson, P., Sothcott, J., Best, A. I., Chapman, M., & Li, X.-Y. (2012), Experimental verification of the fracture density and shear-wave splitting relationship using synthetic silica cemented sandstones with a controlled fracture geometry, *Geophysical Prospecting*, 60(3), 516-525, <https://doi.org/10.1111/j.1365-2478.2011.01021.x>

Tillotson, P., Chapman, M., Best, A. I., Sothcott, J., McCann, C., Shangxu, W., & Li, X.-Y. (2011), Observations of fluid-dependent shear-wave splitting in synthetic

porous rocks with aligned penny-shaped fractures, *Geophysical Prospecting*, 59(1), 111-119, <https://doi.org/10.1111/j.1365-2478.2010.00903.x>

Velcin, H., J. Dautriat, J. Sarout, L. Esteban, and B. Godel (2020), Experimental Reactivation of Shear-fractured Berea and Boise Sandstones by Brine or Liquid CO₂ Injection at Depth, *Journal of Geophysical Research: Solid Earth*, 125(2), e2019JB018281, <http://doi.org/10.1029/2019jb018281>.

Vialle, S., & Vanorio, T. (2011), Laboratory measurements of elastic properties of carbonate rocks during injection of reactive CO₂-saturated water, *Geophysical Research Letters*, 38(1), L01302, <http://doi.org/10.1029/2010GL045606>

Vialle, S., Contraires, S., Zinzner, B., Clavaud, J.-B., Mahiouz, K., Zuddas, P., & Zamora, M. (2014), Percolation of CO₂-rich fluids in a limestone sample: Evolution of hydraulic, electrical, chemical, and structural properties, *Journal of Geophysical Research: Solid Earth*, 119(4), 2828-2847, <https://doi.org/10.1002/2013jb010656>

White, J. E. (1975), Computed seismic speeds and attenuation in rocks with partial gas saturation, *Geophysics*, 40(2), 224-232, <https://doi.org/10.1190/1.1440520>

Winkler, K. W., & Plona, T. J. (1982), Technique for measuring ultrasonic velocity and attenuation spectra in rocks under pressure, *Journal of Geophysical Research: Solid Earth*, 87(B13), 10776-10780, <https://doi.org/10.1029/JB087iB13p10776>

Yin, C. S., Batzle, M. L., & Smith, B. J. (1992), Effects of partial liquid/gas saturation on extensional wave attenuation in Berea sandstone, *Geophysical Research Letters*, 19(13), 1399-1402, <https://doi.org/10.1029/92GL01159>

Accepted Article

Zhou, D., & E. H. Stenby (1997), A Percolation Study of Wettability Effect on the Electrical Properties of Reservoir Rocks, *Transport in Porous Media*, 29(1), 85-98, <https://doi.org/10.1023/A:1006598111378>

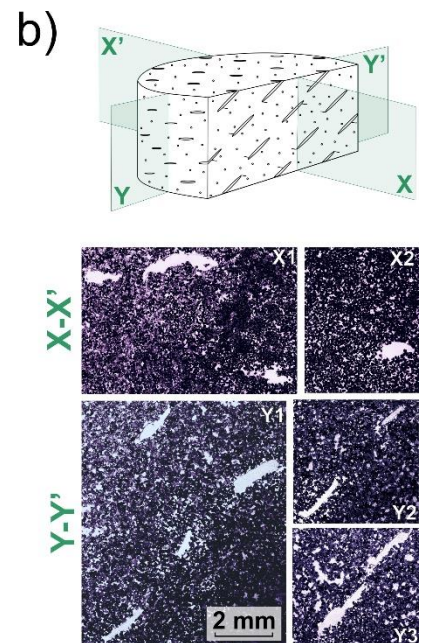
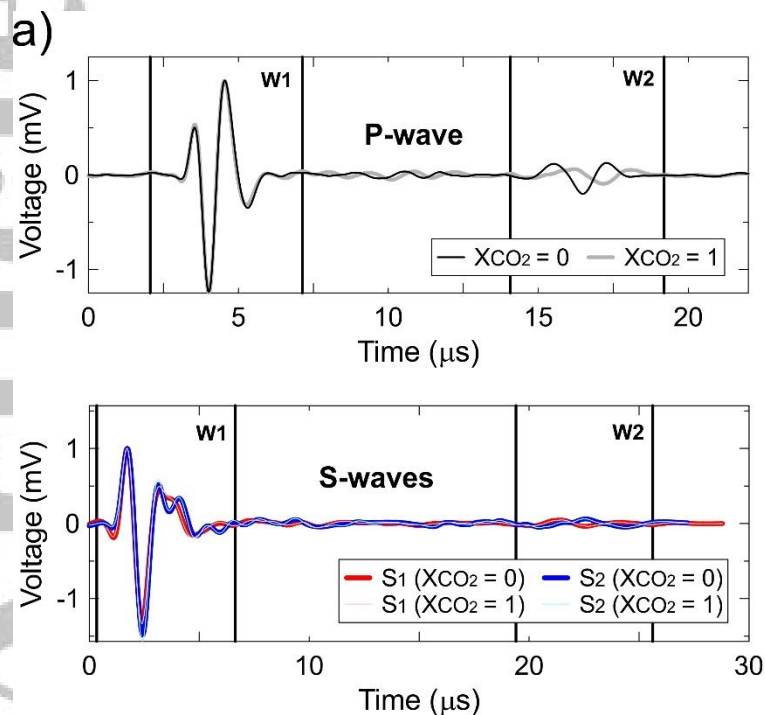


Figure 1. P- and $S_{1,2}$ -wave signals (a) at the saturation states corresponding to fractional flow episodes of pure brine ($X_{CO_2} = 0$) and CO_2 ($X_{CO_2} = 1$). W1 and W2 indicate the time windows used for Fourier analysis (Best, 1992). (b) Thin section analysis from two (mutually orthogonal) slides prepared after the BCFT test. From original images, colour channel filtering was applied to emphasize porous (bright) with respect to grains (dark) areas.

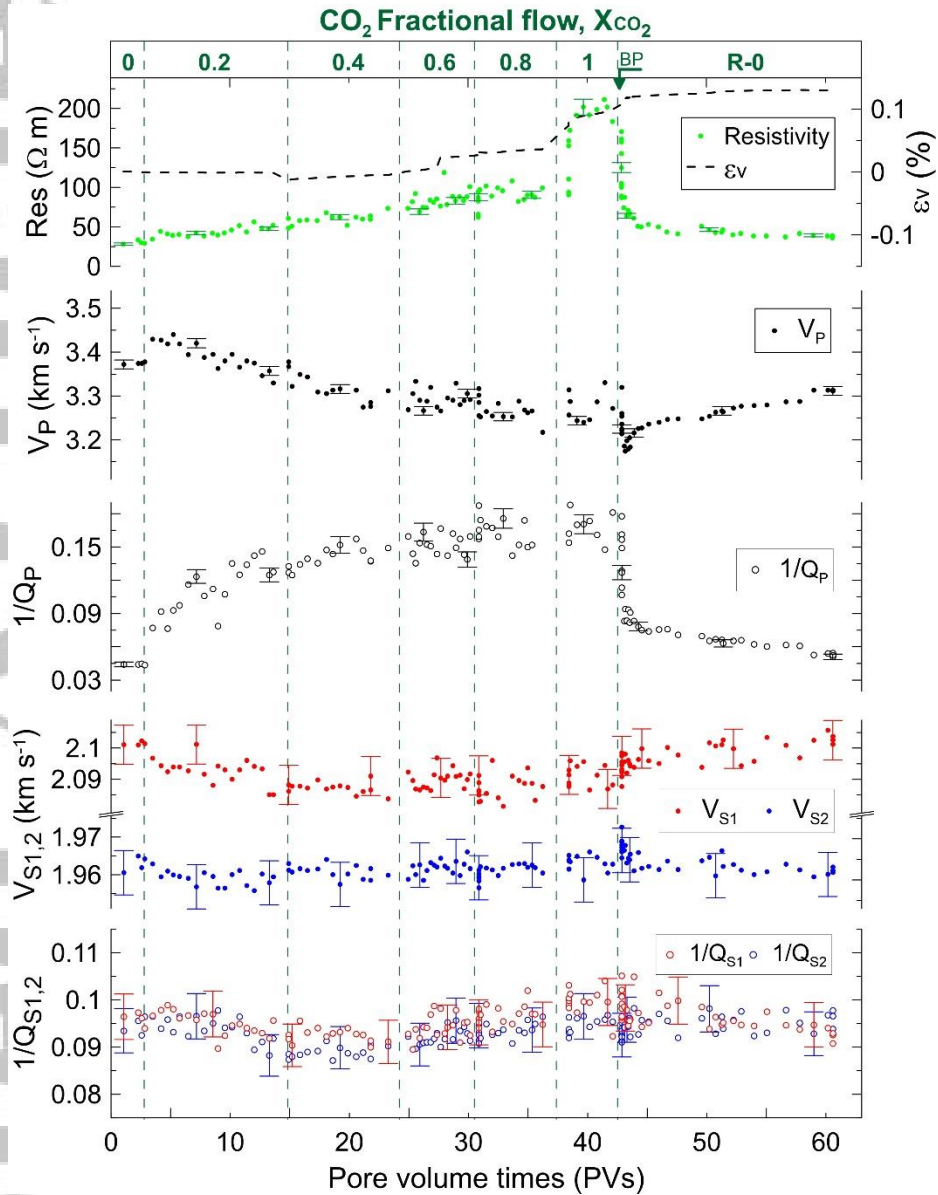


Figure 2. Brine-CO₂ flow-through test in fracture sandstone. P- and S_{1,2}-wave velocities (V_P , $V_{S1,2}$), attenuations (Q_P^{-1} , $Q_{S1,2}^{-1}$) and electrical resistivity, together with volumetric strains for six brine:CO₂ flow rates drainage episodes ($X_{CO_2} = 0$ to 1) and the forced imbibition ($X_{CO_2} = R-0$; BP denotes the initial imbibition brine pulse; see text). The ultrasonic properties were measured at a single frequency of 600 kHz (pulse-echo technique), obtained from Fourier analysis of broad band signals. Error bars displayed every 10 measurements.

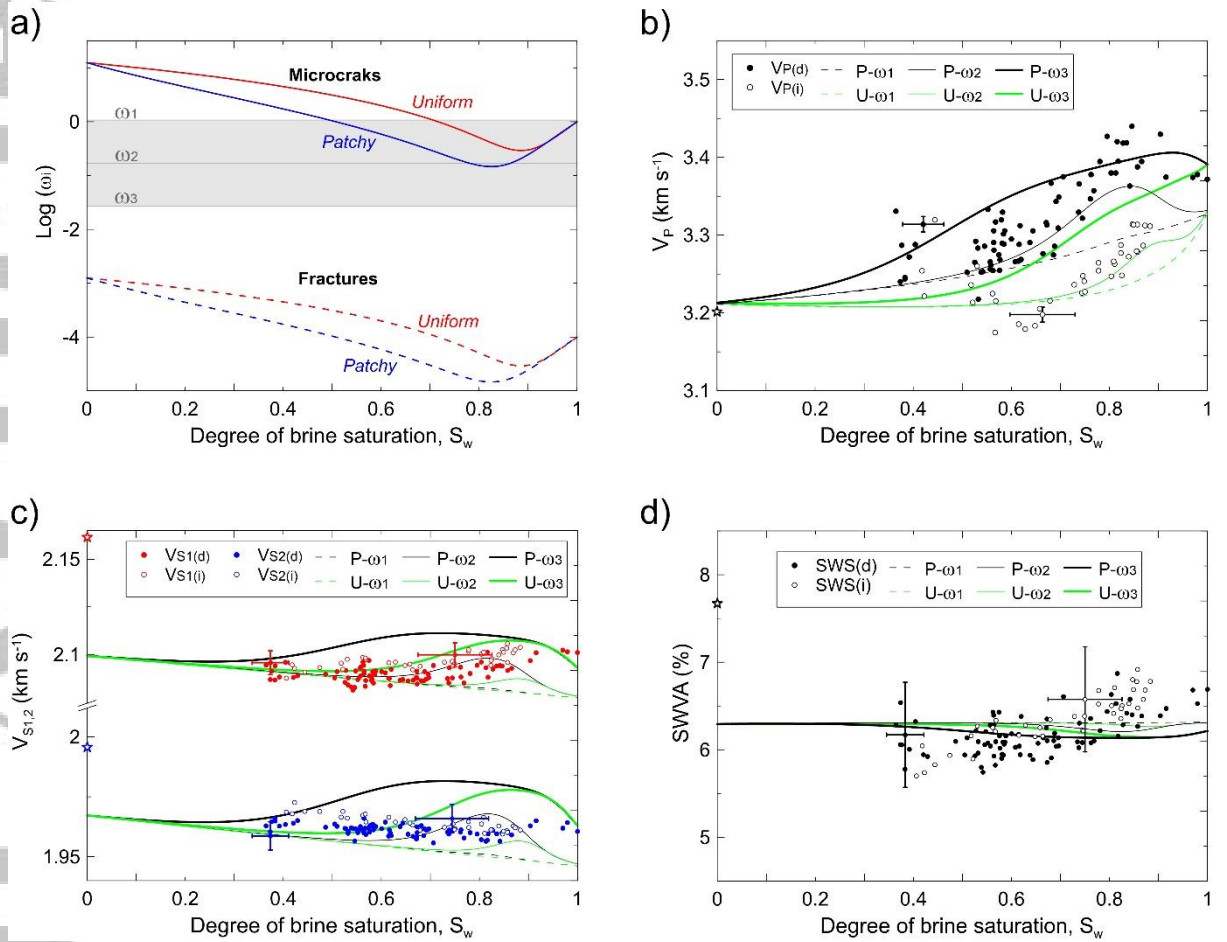


Figure 3. (a) Patchy and Uniform models for microfractures and fractures frequency domains. Ultrasonic P- and S-wave velocities V_p (b), and V_{S1} and V_{S2} (c), and S-wave velocity anisotropy, $SWVA = (V_{S1} - V_{S2}) / V_{S1} \times 100$ (d), versus degree of brine saturation (S_w). Two modelling scenarios for pore fluid distribution: uniformly (U, with patch parameter $q = 1$), and patchy (P, with $q = 0.2$), at frequencies $\omega_1=0.027$, $\omega_2=0.17$ and $\omega_3=1.0725$. Subscripts d and i refer to drainage and imbibition, respectively. The star symbol indicates the CO_2 saturation measurement (see text). Two single cross bars show horizontal and vertical errors for low and high S_w .